Journal of Molecular Liquids 386 (2023) 122492

Contents lists available at ScienceDirect

Journal of Molecular Liquids

journal homepage: www.elsevier.com/locate/molliq

Interfacial structure of protic and aprotic ionic liquid-DMSO-Li salt mixtures near charged and neutral electrodes: A Molecular Dynamics study

Martín Otero-Lema [a,b,1], Pablo Martínez-Crespo [a,b,1], Trinidad Méndez-Morales [a,b], Hadrián Montes-Campos [a,b,c,*], Luis M. Varela [a,b,*]

[a] Grupo de Nanomateriais, Fotónica e Materia Branda, Departamento de Física de Partículas, Facultade de Física, Universidade de Santiago de Compostela, Campus Vida s/n, Santiago de Compostela, E-15782, Galicia, Spain

[b] Instituto de Materiais (iMATUS), Universidade de Santiago de Compostela, Campus Vida s/n, Santiago de Compostela, E-15782, Galicia, Spain

[c] CIQUP, Institute of Molecular Sciences (IMS)—Departamento de Química e Bioquímica, Faculdade de Ciências da Universidade do Porto, Rua Campo Alegre, 4169-007, Porto, Portugal

ARTICLE INFO

Keywords:
Ionic liquids
Structure
Molecular Dynamics
DMSO
Implicit interfaces
Ternary mixtures

ABSTRACT

In this paper we report classical Molecular Dynamics simulations of the interfacial structure of two ternary mixtures, based on both a protic (ethylammonium nitrate, EAN) and an aprotic (1-ethyl-3-methylimidazolium tetrafluoroborate, $EMIMBF_4$) ionic liquid. A molecular solvent (dimethylsulfoxide, DMSO) and a lithium salt with common anion are the rest of the components of the mixtures. The simulations were performed with implicit graphene walls, both neutral and charged with a surface charge density of ± 1 e/nm^2. Density, charge and electrostatic potential profiles as well as integral capacitances were calculated for all systems. For both liquids, the evolution of the density profiles throughout the DMSO concentration range are in accordance with previously characterized bulk properties of such systems. In the case of charged interfaces, the adsorption of Li^+ cations into the negative electrode was found to be possible for the protic liquid, but unfavourable in the case of the aprotic one. Moreover, the probability distribution functions for the orientation of all molecular species near the interfaces were computed, and they indicate a tendency of the solvent molecules to form a dense layer at the interface separating the ionic liquids from the electrodes. The influence of hydrogen bonds in determining the dissimilitudes between protic and aprotic mixtures is highlighted.

1. Introduction

A rise in the frequency of extreme climatic phenomena due to the excess of greenhouse gases has been experienced in the last decade [1,2], from which derives a need for clean, alternative energy sources. Renewable power generation with photovoltaic panels and wind turbines - among others - and electric mobility are being key in this transition from fossil fuels. The performance of the first is nevertheless dependent on atmospheric conditions, which inevitably makes energy storage a requirement to both ensure the coverage of the power demand on electric grids and the appropriate functioning of vehicles [3–6]. Besides, an increasing demand for portable and more powerful electronic devices is being experienced, which further brings up the need for efficient electrochemical energy storage [7,8].

Electrochemical devices are nowadays the most commonly used technology to store energy which is to be turned into electricity. Furthermore, they are employed in several processes of industrial and environmental interest such as CO_2 capture [9–11], production of fertilizers [12–15] and water electrolysis for hydrogen fuel cells [16,17]. Alas, our understanding of their operating laws is limited. This hinders the development of improved devices and methods for the aforementioned ends. Researching the fundamental physico-chemical working principles of materials is crucial nowadays to guarantee the accomplishment of this required change of ecologic paradigm. Those principles are fundamental for determining the properties of interest for each utility.

The suitability of a material for any specific usage strongly depends on its molecular ordering. A matter of special interest for electrochemical devices entails the structure at electrode interfaces, which cannot

* Corresponding authors at: Grupo de Nanomateriais, Fotónica e Materia Branda, Departamento de Física de Partículas, Facultade de Física and Instituto de Materiais (iMATUS), Universidade de Santiago de Compostela, Campus Vida s/n, Santiago de Compostela, E-15782, Galicia, Spain.
E-mail addresses: hadrian.montes@usc.es (H. Montes-Campos), luismiguel.varela@usc.es (L.M. Varela).
[1] Contributed equally to this work.

https://doi.org/10.1016/j.molliq.2023.122492
Received 8 March 2023; Received in revised form 2 June 2023; Accepted 30 June 2023
Available online 5 July 2023

be experimentally accessed straightforwardly. In this regard, computer simulations at the atomic scale may provide a valuable insight into the foundations of the matter [18,19]. A high degree of control of the parameters ruling the interactions of the systems in study is achieved with this procedure. Moreover, contrast of results with experiments usually results in valuable, reciprocal feedback [20]. *Ab initio* methods are expected to provide exact results within chemical accuracy [21], but their high computational cost precludes their applicability for exploring the properties of systems with a large number of atoms. Molecular Dynamics (MD) simulations based on model Potential Energy Surfaces adjusted to *ab initio* or experimental parameters stand as an optimal alternative in terms of efficiency-accuracy balance [22].

Ionic liquids (ILs) are among the most remarkable candidates for the next generation of energy solutions. They are room temperature molten salts usually made up of a bulky organic cation and an inorganic anion [23], which hinders crystal packing and keeps a low melting temperature. A set of appealing features such as wide electrochemical windows, nonvolatility and non-flammable nature provide them with desirable properties for their employment in safe electrochemical devices [24–26]. However, most modern electrochemical storage devices rely on the transport of metallic cations from the bulk electrolyte to the cathode, such as the widespread lithium-ion battery [27]. In the case of pure ILs as electrolytes, transport of Li^+ is hindered by their low transference number and high viscosity.

These issues fundamentally arise from the fact that ILs are tightly bound by the long range Coulomb interaction. They can be addressed by mixing the IL with a molecular solvent, in which is called a binary mixture. As the solvent replaces charged ions in the mixture, the influence of the electrostatic interaction within the system decreases. This causes the molecules to diffuse more freely in the mixture, which in turn improves the transport properties of these binary systems. The properties of binary mixtures have been thoroughly studied both experimentally [28–30] and computationally [31–33]. Moreover, extensive theoretical work has been carried out in order to characterize the underlying mechanism for transport phenomena in these systems, such as the pseudolattice (or Bahe-Varela) theory [34] and the random-alloy model for electric conductivity [35].

Recently, ternary mixtures of ILs with a solvent and a salt have been proposed as a compelling option as electrolytes for electrochemical energy storage. Addition of organic solvents to reduce the coordination of Li^+ with the anions has been shown to enhance Li^+ transport number in the bulk [36]. Oldiges et al. [37] already proved this fact for two salts in several ILs with organic solvent mixtures.

In a previous work carried out by the authors in Ref. [38], a ternary mixture of a protic IL and one of an aprotic IL with dimethyl sulfoxide (DMSO) - an organic solvent receiving growing interest due to its low reactivity and high miscibility [39,40] - and lithium salts were studied. Ethylammonium nitrate (EAN) and 1-ethyl-3-methylimidazolium tetrafluoroborate ($EMIMBF_4$) were the protic and aprotic ILs of choice, respectively. Lithium salts were comprised of Li^+ and the corresponding anion of the IL. Clear differences were found among the structure and dynamics depending on whether the employed IL was protic or aprotic. The coordination numbers and electrical conductivity of every mixture were computed throughout the whole solvent concentration range. In both cases, the results were indicative that the composition of the solvation shell of the metal cations in the mixtures and the rate at which anions in it were replaced by DMSO molecules were the major features determining the change of conductivity with solvent molar fraction. Furthermore, it was observed that $[EA]^+$ forming hydrogen bonds - a common phenomenon in protic IL mixtures [41–43] - with DMSO prevented the solvent from substituting the anions in the Li^+ solvation shell. These features led to an abrupt rise in conductivity in the protic mixture for 60% DMSO molar fraction due to disruption of the hydrogen bond network, whereas the conductivity of the aprotic mixture grew gradually.

Regarding interfaces, Li et al. [44] found that ternary mixtures of ILs with a solvent and a salt could lead to lithium metal anode stabilization. Despite the relevance of these mixtures, the authors had no knowledge of MD reports about their properties near neutral and charged interfaces so far. Therefore, in the present contribution we aim at expanding the insights obtained from the mentioned previous bulk study of these systems. To this end, MD simulations of the same mixtures subjected to confinement between implicit graphene walls were performed, both with neutral and charged walls.

The structure of the paper is as follows. In Section 2, the settings of the simulations are thoroughly detailed. Section 3 is devoted to the description and discussion of the density, orientation and charge profiles as well as to an analysis of the electrostatic potential of the mixtures. Finally, the conclusions of the work are exposed in Section 4.

2. Methodology

In this work, several MD simulations were performed to study the properties of ternary mixtures of solvent + IL + Li^+ salt. As previously mentioned, EAN and $EMIMBF_4$ were chosen as ILs in order to gauge the differences in the behaviour of protic and aprotic ILs when subjected to confinement between implicit graphene walls. DMSO was the common solvent for both ILs, whereas $LiNO_3$ and $LiBF_4$ were the salts for the protic and aprotic ILs, respectively. The mixtures were studied throughout a wide solvent concentration range for the neutral walls, while only concentrations from 70% upwards were simulated in the presence of charged walls due to slow, crystal-like diffusion in the other cases.

All systems were simulated using the GROningen MAchine for Chemical Simulations (GROMACS) version 2020.4 [45]. The chosen force field was the Optimized Potentials for Liquid Simulations in its all-atom version (OPLS-AA) [46,47]. The force field parameters for each individual molecule were the same as the ones reported in Ref. [38]. A constant molar fraction of 7.5% of the corresponding lithium salt was used for all simulations.

For all simulations, temperature was held constant using a velocity-rescale algorithm [48] with a coupling time of 0.1 fs. When pressure coupling was employed, it was through the use of a Parrinello-Rahman semi-isotropic barostat [49,50]. The compressibility in the xy directions was set to be that of water, and the one in the z direction was chosen to be zero so as to ensure that the length in that direction remained the same for all simulations. System size in the z direction was set at 10 nm. Coupling time for the barostat was set to 1 fs. Periodic boundary conditions were enforced in the x and y directions, following the natural symmetries of the systems at hand. The electrostatic potential energy was computed using smooth Particle-Mesh Ewald (PME) electrostatics [51] with a real space cut-off radius of 1.1 nm, whereas Fourier grid spacing was 0.12 nm with cubic interpolation. For all systems, adequate slab geometry corrections [52] were carried out in the Ewald summations in order to account for the semiperiodicity of the system. Finally, a cutoff radius of 1.1 nm was used to deal with van der Waals forces, and the corresponding long range corrections to the energy and pressure were taken into account.

Regarding the walls, implicit interfaces like the ones used in Ref. [53] were employed instead of simulating an interface consisting of individual atoms. This consist in replacing the atomic structure of the electrode with a 10-4 Lennard-Jones (LJ) potential. This potential is the result of integrating the interaction of an homogeneous distribution of atoms interacting with a 12-6 LJ potential. The LJ parameters of the wall were set to those of the carbon atoms in benzene (opls-145) following the same reference. The number density of the mass distribution was chosen to be 38.18 nm^{-2} to match that of graphene.

In order to properly compare the results, the simulation procedure was the same for both ILs and all DMSO concentrations. First, simulation boxes were created with PACKMOL [54]. The total number of molecules was set to 2000 in every simulation, with a total of 150 salt molecules present in each simulation. All simulation boxes were set to

have the same length in the z direction - perpendicular to the interfaces - for greater ease of comparison between concentrations. The box sizes in the x and y direction differed for each box, and were set to accommodate each individual concentration.

Once the simulation boxes were created, energy minimization was carried out in GROMACS using a steepest descent algorithm with a 0.1 kJ mol^{-1} nm^{-1} tolerance and an initial step of 0.01 nm. After the energy minimization, an annealing process was carried out in the NpT ensemble for a total of 13 ns, consisting in five distinct steps. Firstly, a 1 ns period where the temperature was held constant at 298.15 K, followed by a 0.5 ns window when the temperature linearly rose to a value of 600 K. The system remained at that fixed temperature for 1 ns, to then undergo a linear decrease of temperature back to the original 298.15 K value, again within a 0.5 ns window. Finally, the system evolved during 10 additional nanoseconds at 298.15 K. During the process, pressure was held at a constant value of 1 atm, and a timestep of 1 fs was employed. Afterwards, a stabilization in the NVT ensemble was carried out for 10 ns, with a bigger timestep of 2 fs and a temperature of 298.15 K. Finally, production runs in the NVT ensemble were performed at the same temperature using the same timestep for a total of 20 ns.

2.1. Charged interfaces

The effects of a constant charge distribution were modeled by introducing an external electric field calculated to be the same as the one generated by a capacitor with a surface electric charge density of ±1 e/nm^2, as detailed in Ref. [53]. From direct integration of the Poisson equation, the value of the electric field was estimated to be 18.18 V/nm. The initial configurations for these simulations were the final ones for non-charged implicit interfaces. Once the external field was introduced, a stabilization in the NVT ensemble was carried out for 20 ns, followed by 30 ns production runs also in the NVT ensemble. These production runs were larger than the previous ones in order to better capture the slow processes that take place under the effects of the electric field. For both stabilization and minimization a timestep of 2 fs was used. These simulations were not carried out through the whole concentration range, and rather only for high DMSO concentrations of 70% and above. These concentrations were shown to be sufficiently high for the hydrogen network present in EAN to be disrupted by the solvent [38]. This way, the slow dynamics that results in the protic mixtures behaving as quasi-solids - which would require larger stabilization runs - was avoided.

3. Results and discussion

3.1. Density profiles

To analyze the structure and composition of the molecular layers near neutral interfaces, number densities of an atom from each chemical species were computed along the z-axis of the box for all DMSO molar fractions of each mixture. These were normalised to the average density in the bulk, considered for z between 2 and 8 nm, and are shown in Fig. 1. In the $EMIMBF_4$ mixtures, densities of chemical species were obtained from the positions of nitrogen atoms bonded to the ethyl chain and boron atoms in the $[EMIM]^+$ and $[BF4]^-$ ions, respectively. Meanwhile, nitrogen atoms from both the $[EA]^+$ and $[NO_3]^-$ ions were selected in the EAN mixture. The sulfur atom from DMSO was chosen in every case. Obviously, the ion itself was chosen for Li^+ number density.

For Li^+ ions, a vague layered structure may be appreciated in the $EMIMBF_4$ mixture, which is depicted by the peaks being around the same positions for all molar fractions. In contrast, it is easily seen that the distribution of Li^+ in the EAN mixture lacks that ordering and reveals a slight depletion of Li^+ from the bulk when DMSO concentration is raised. A similar tendency may be recognized for the IL cations. While the layer structure is maintained in the $EMIMBF_4$ mixtures throughout the whole DMSO concentration range, layers get distorted in the EAN mixtures. Nevertheless, a well defined first layer of cations is placed at about 5 Å from the walls in both cases. Furthermore, $[EMIM]^+$ molecules exhibit a manifest preference for staying close to the walls, with ions shifting from the bulk towards the interfaces for the higher DMSO molar fractions. This is a common trend in nonpolar ions [55], and could be responsible for the lack of Li^+ near the walls in the aprotic mixture.

Contrarily to the positive ions, IL anions are acknowledged to keep similar behaviours in both mixtures. Likewise to the anions, the DMSO density distributions for both IL mixtures are not very distinct from one another. A marked tendency to stay near the walls is displayed, which would not be desirable for electrochemical devices due to potential damages that DMSO migrating towards the electrodes could cause if unwanted chemical reactions took place. However, one of the remarkable attributes of DMSO as a solvent is its wide electrochemical window [56], which makes it less reactive and thus reduces the risk of degrading the battery cell.

To study how the molecular structure of the mixtures changes under the presence of a charged interface, the same atoms were selected for the normalised number densities of each chemical species. The resulting distributions are displayed in Fig. 2.

No remarkable differences are observed between the different mixtures for the anion and solvent distributions. Nevertheless, the density profiles for the positive ions do display dissimilitudes among both IL mixtures. On the one hand, for Li^+ we have quite differing maxima evolution with solvent concentration. The EAN mixture allows Li^+ to approach both walls more easily, whereas the negatively charged wall is clearly preferred in the $EMIMBF_4$ one. On the other hand, the nonpolar nature of $[EMIM]^+$ compared to $[EA]^+$ is certainly visible from the heights of the peaks in both distributions, with a much higher tendency of $[EA]^+$ to deplete the bulk zone.

Finally, in the case of EAN and for DMSO concentrations of 80 and 90%, a Li^+ peak is observed at a distance of 2 Å from the negatively charged interface. These peaks correspond to Li^+ ions that managed to cross the DMSO layer present at 3 to 5 Å from the electrode and now lay in a stable point next to the implicit interface, as depicted in Fig. 3. This indicates the presence of an energy barrier that the metallic cations have to surpass in order to traverse the DMSO layer. This barrier cannot be explained solely on the basis of electrostatic energy, as will be made apparent later, and thus its nature has to depend on both chemical and dynamical factors. Moreover, the fact that these adsorbed Li^+ ions were not found for every concentration hints at the fact that this state of the lithium cations could be unstable and that they could return to the major Li^+ layer placed at 5 Å from the electrode, where a more stable energy minimum is located. The adsorption of Li^+ at the interface could be an effect of the initial packing of the system. However, we verified that no Li^+ were there at the beginning of the simulation and that they were able to cross the energy barrier several times during the simulation. Moreover, similar results for protic ILs enhancing the adsorption of Li^+ at the electrode has already been reported by Gómez-González et al. [57]. They report that the underlying mechanism consists in the Li^+ ion being coordinated with at least one anion and that allows to the Li^+ to go through the positively charged layer of IL cations. This image is congruent with our previous results for bulk systems where we found that at high DMSO concentration Li^+ ions are always coordinated with at least one NO_3^- anion in the protic IL while there are no $BF4^-$coordinating anions in the aprotic IL. Therefore, this could explain the different behaviour of both ILs.

Generally, all chemical species recover their bulk density for a lower DMSO fraction in the $EMIMBF_4$ mixture than in the EAN mixture. This seems to be due to the better fluidification of $EMIMBF_4$ as DMSO is added, something characteristic of these mixtures in the bulk regime [38]. The oscillations in the density distributions of the protic mixtures are expected to be caused by the hydrogen bond network hindering substitutions in the solvation shells. Both systems show that less densely

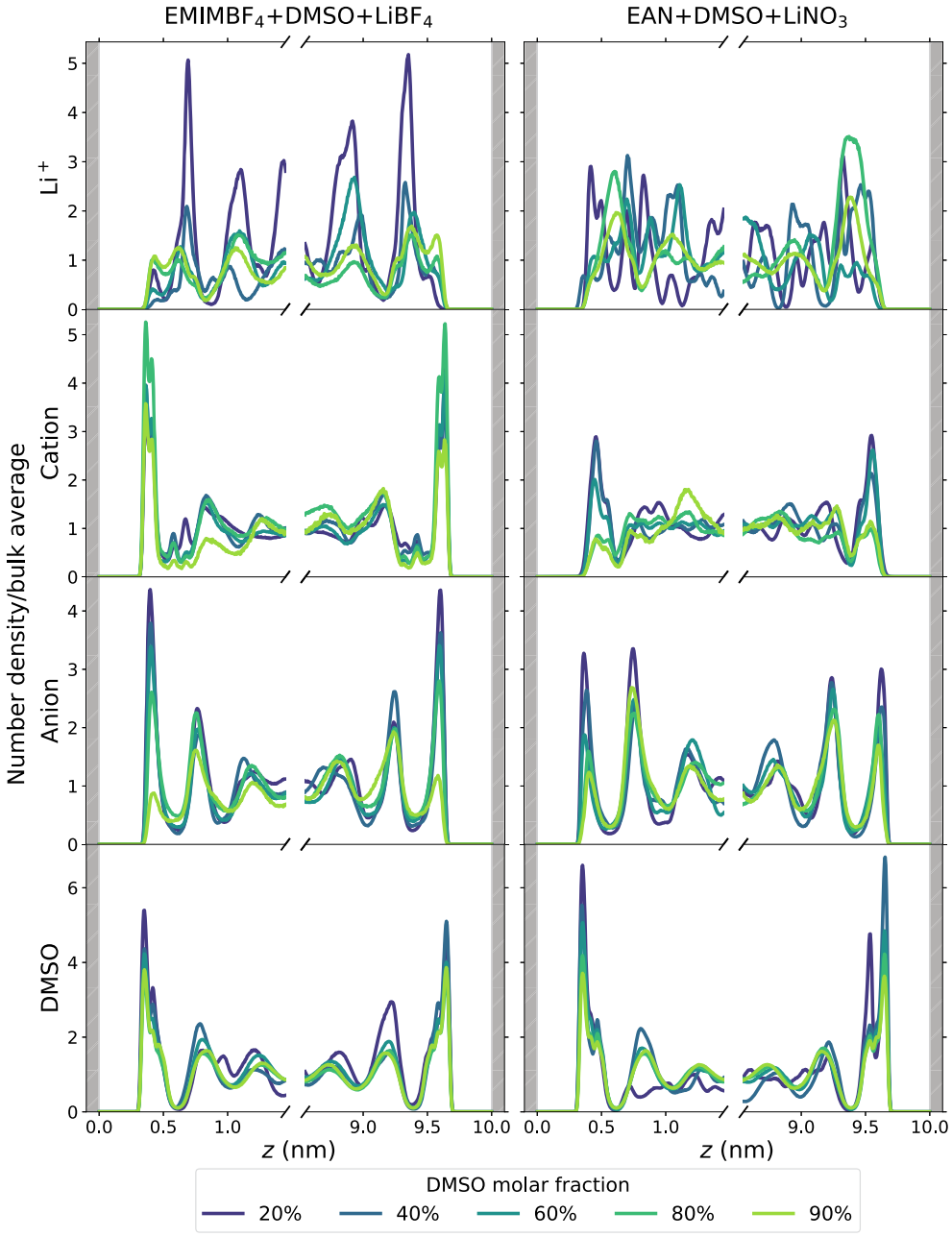

Fig. 1. Number densities along the z-axis for all chemical species near the neutral walls normalised to the average number density in the bulk of said species.

charged species (i.e. $[EMIM]^+$ and DMSO) have higher tendency to deplete the bulk and position themselves near the interfaces, where a complex layered structure is present.

Under the effect of an electric field, the density distributions differ significantly from those for neutral walls. The resulting layer structures are unaltered by the variation in DMSO concentration. Thus, the electric field is overtaking hydrophobic effects arising from molecular interactions as the driving force for the layering. DMSO molecules having strong dipolar moment make them retain their preference for the interfaces. This results in the formation of a molecular barrier that Li^+ cations have to surpass in order to reach the electrodes, which they are capable of doing in the protic IL mixtures. This is again in accordance with the bulk behaviour of the systems, where Li^+ cations showed higher mobilities in the protic IL [38]. For energy barriers of the same height, a greater mobility will result in more collisions with the barrier, increasing the probability of getting across it. Furthermore, H-bond interaction between $[EA]^+$ and DMSO could also participate in the interplay to modify the structure and promote Li^+ surpassing of the barriers.

3.2. Orientational order

The orientations of molecules within the first 5 Å of distance to the electrodes were computed for both neutral and charged interfaces. These contain the orientational order within the electric double layer, since it was found that beyond that distance an homogeneous probability distribution is reached.

In Fig. 4 the probability density distribution of the cosine of the angle between a vector perpendicular to the interfaces and a characteristic vector for each molecule are represented for non charged interfaces. The characteristic vectors were chosen as follows. $[EA]^+$: the vector originating from the nitrogen atom that points to the geometric centre of the hydrogen atoms bonded to it. $[NO_3]^-$: the vector originating from the nitrogen atom pointing perpendicular to the plane defined by

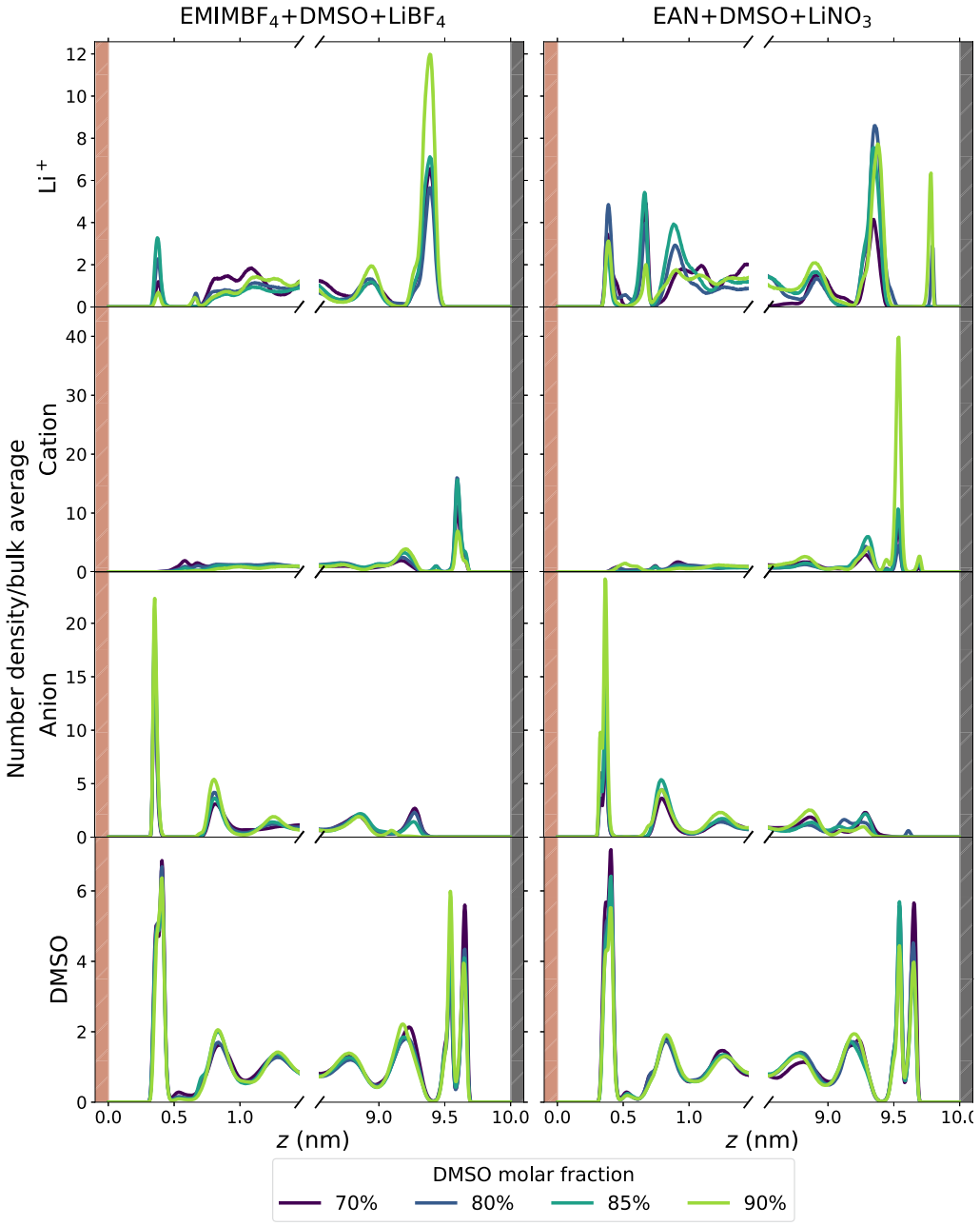

Fig. 2. Number densities along the z-axis for all chemical species near the charged walls normalised to the average number density in the bulk of said species. Positive wall is red-coloured, negative wall is black-coloured.

the molecule. $[EMIM]^+$: the vector originated in the geometrical centre of the imidazolium ring, pointing in the direction perpendicular to it. $[BF4]^-$: the vector along the direction of one of the B-F bonds. DMSO: the vector pointing in the direction of the S-O bond. These characteristic vectors are displayed in Fig. 4.

It can be seen that both EAN and $EMIMBF_4$ cations present a robust orientational structure that is not perturbed by the addition of DMSO to the mixture. $[EMIM]^+$ cations show a clear reflection symmetry expected from the geometry of the species, presenting a preference for orientating the imidazolium ring parallel to the interface. This effect was already found by Rajput et al. [58] for pure EMIMTFSI confined by graphene walls with the same separation. Interestingly, in Ref. [59] it is reported that in the case of pure $EMIMBF_4$ and for a smaller distance between the interfaces (ranging from 10 to 28 Å), the imidazolium ring did not show such a strong interaction with the interface. Instead, the alkyl chain of the cation was placed closer to the walls, with the ring orientated perpendicularly to the interfaces. Thus, the orientational order of IL cations near the interface is shown to greatly depend on the confinement level of the mixtures. On the other hand, $[EA]^+$ cations show two distinct favourable orientations, one sharp peak representing the polar head pointing to the interface and a wider distribution representing that head orientated towards the bulk.

Anions show a stronger response to variations in DMSO concentration in both the protic and aprotic IL mixtures. For low DMSO molar fractions, both anions show a clear orientational preference. $[NO_3]^-$ anions tend to align their molecular planes with the interface, whereas $[BF4]^-$ anions orientate the base of the tetrahedral complex towards the interface. In both cases, the probability density flattens once DMSO concentration is increased, signalling the loss of orientational ordering. Interestingly, $[NO_3]^-$ anions develop a new orientational preference consisting of a 90° rotation from the previous ones, corresponding to

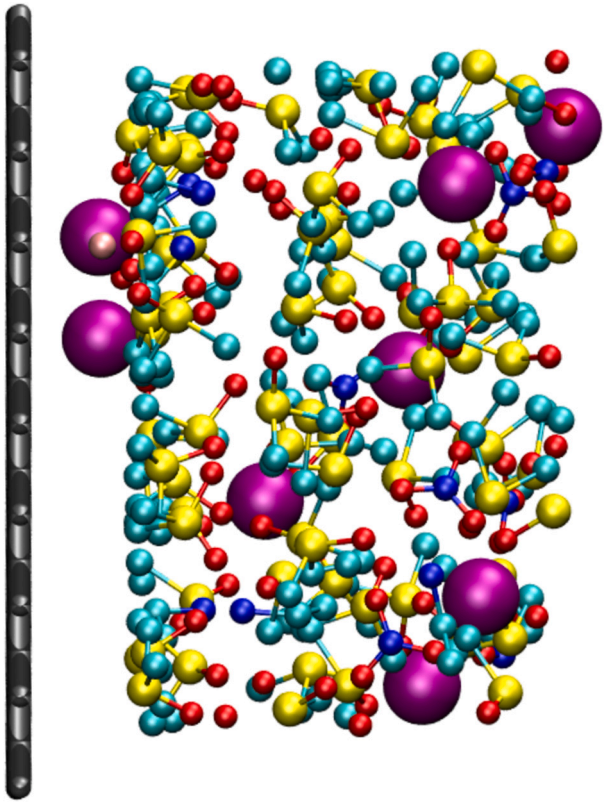

Fig. 3. Snapshot of adsorbed Li^+ cations taken from the final configuration of the EAN simulation at 90% DMSO concentration. The size of the metal cations (purple) is greatly enlarged for clarity purposes. Hydrogen atoms have been omitted. The implicit negative electrode has been represented as black bonds for clarity too.

the anions orientating their molecular plane perpendicular to the interfaces for high DMSO concentrations.

Finally, a clear difference in the orientational structure of solvent molecules can be seen between the protic and aprotic IL. For high DMSO concentrations, similar probability distributions are found. These depict DMSO molecules pointing their oxygen atom towards the bulk, favouring the appearance of a thin electropositive layer near the interfaces due to the positively charged hydrogen atoms in the solvent molecules. However, in the case of the protic IL it can be seen that a peak around $\cos\theta = 0.75$ is developed for low DMSO concentrations, corresponding to the oxygen atom in DMSO pointing to the bulk. This peak gradually decreases as DMSO concentration is raised, but even for high DMSO concentrations it remains higher than the corresponding one for $EMIMBF_4$.

This difference between the two liquids can be explained by the protic nature of EAN. As previously reported in Ref. [38], the hydrogen atoms bonded to the nitrogen atoms in $[EA]^+$ cations form hydrogen bonds with the electronegative oxygen atoms in DMSO molecules. From the orientational order of $[EA]^+$ cations, it can be seen that they exhibit a preference for orienting the nitrogen atom towards the interface. Thus, in order for a hydrogen bond to be formed between cations and solvent molecules, it is required that the oxygen in DMSO aligns itself with the N atom in $[EA]^+$. This results in the S-O bond orienting itself towards the bulk. This effect is not present in $EMIMBF_4$ due to its aprotic nature, and thus that peak does not show a relevant dependence with DMSO concentration.

The results obtained for neutral interfaces are in good agreement with the density profiles presented in the previous section. The affinity of $[EMIM]^+$ cations to place themselves near the interfaces is displayed in the orientation of the first layer, where those molecules tend to align with the walls. In both liquids, DMSO shows a richer orientational

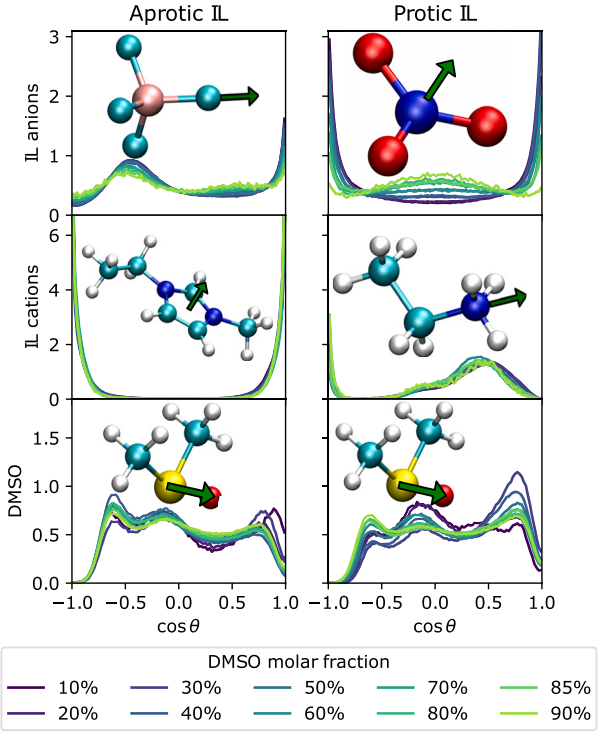

Fig. 4. Probability density distributions of the cosine of the angle between a vector perpendicular to the neutral interfaces and the characteristic vector for each molecule, represented inside of each plot. The characteristic vector of each molecule is represented by a green arrow.

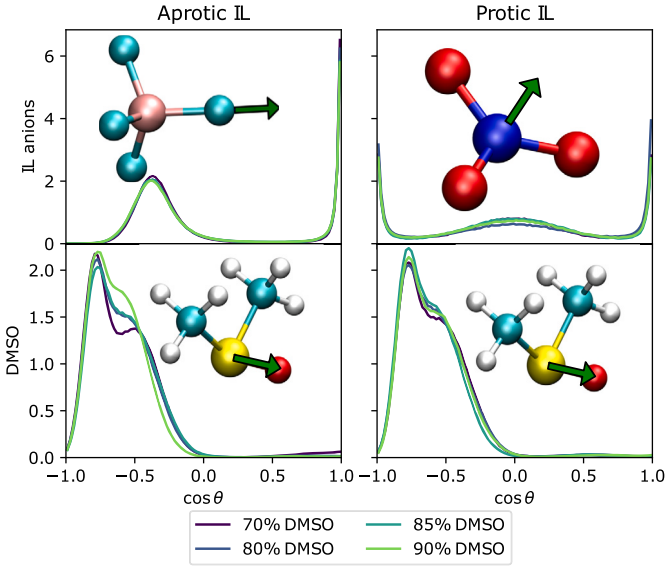

Fig. 5. Probability density distributions of the cosine of the angle between a vector perpendicular to the positive interfaces and the characteristic vector for each molecule, represented inside of each plot. The characteristic vector of each molecule is represented as a green arrow.

structure than the ions, which often only have a couple of preferred orientations, whereas the solvent seems to be more lenient in this regard. This is consistent with the fact that the DMSO layer near the interfaces is much wider than those for the other species. A wider layer accommodates more molecules, and thus interactions among those molecules can result in a rich variety of orientations. This is not the case for thin layers, where the interaction with the walls dominates and thus results in a few preferred orientations.

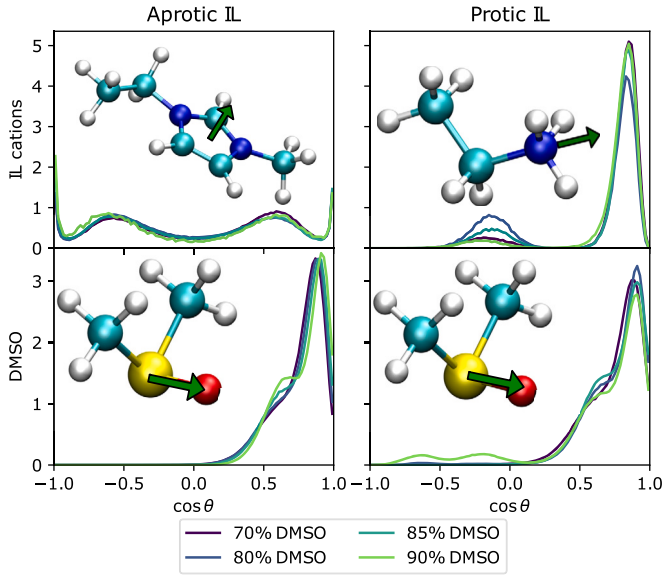

Fig. 6. Probability density distributions of the cosine of the angle between a vector perpendicular to the negative interfaces and the characteristic vector for each molecule, represented inside of each plot. The characteristic vector of each molecule is represented as a green arrow.

For the charged systems, in Figs. 5 and 6 the probability density distributions for the positively and negatively charged interface, respectively, are represented. Only the orientation of the species with the highest concentration in each region are represented, since the low concentration of anions (cations) in the negative (positive) interface leads to insufficient statistical accuracy. For the positive interface (Fig. 5), it can be seen that the orientational structure is very robust with respect to variations in solvent concentration. This again implies that, when present, the external electric field takes over from the intermolecular interactions as the driving factor behind the microscopic structure of the molecular layers.

In both cases, DMSO molecules orientate their negatively charged oxygen atom towards the interface, in a wide range of orientations. As for the anions, $[BF4]^-$ shows the same tendency that was observed for low solvent concentrations between non charged walls, orientating the base of the tetrahedral parallel to the wall, while $[NO_3]^-$ anions present again two preferred orientations differing in a 90° rotation, with the molecular plane either parallel or perpendicular to the interface.

A similar behaviour can be seen in the negatively charged interface showing no, major changes with variations in DMSO concentration. In the case of $EMIMBF_4$, $[EMIM]^+$ cations show two distinct orientations (taking into account the symmetries of the ring): the imidazolium ring parallel to the interfaces - a behaviour already observed for the neutral walls - and a secondary orientation around $\cos\theta = \pm 0.5$ corresponding to the imidazolium ring being slightly tilted.

For both ILs, DMSO molecules show a clear preference to orientate their oxygen atoms away from the interface, facing their positively charged hydrogen atoms towards the interface, which can be seen in Fig. 3. Finally, for the protic cations, some differences can be seen as DMSO concentration varies. While $[EA]^+$ cations show a tendency to point their polar heads towards the bulk, which again results in the formation of a layer of hydrogen atoms near the interface, a secondary orientation can be seen around $\cos\theta \simeq -0.2$, corresponding to the C-N bond being almost parallel to the implicit interface. This peak is found for the intermediate simulated DMSO concentrations, while for the extremes it does not appear to be as prevalent.

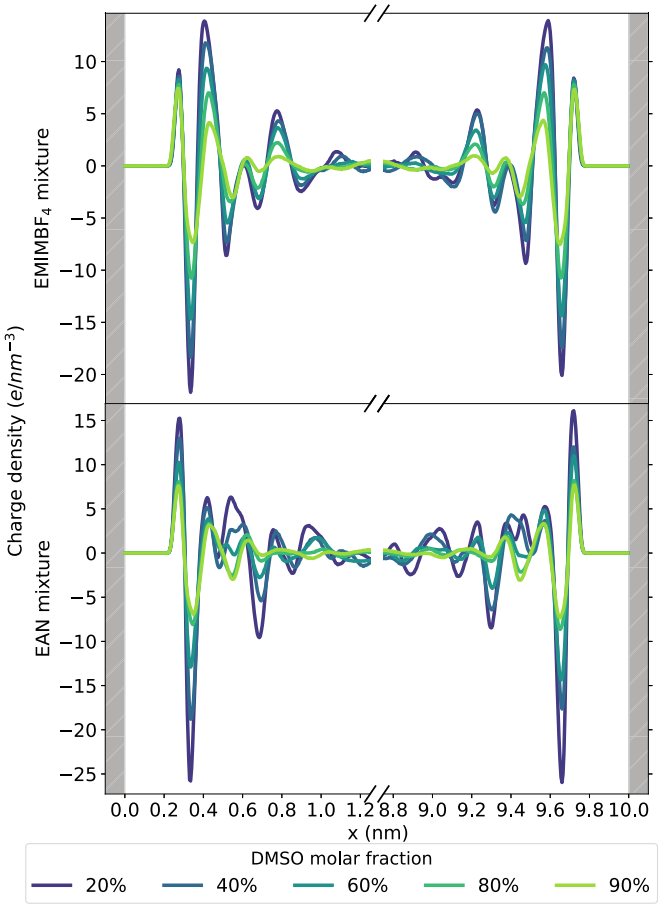

Fig. 7. Charge densities along the z-axis for both mixtures without an external field.

3.3. Charge profiles

Charge density distributions of both mixtures with neutral walls along the z-axis are shown in Fig. 7. The extrema in both distributions reveal that the layer structure is better preserved along the DMSO concentration range in the $EMIMBF_4$ mixture. In contrast, the charge layers in the EAN ternary mixture suffer a displacement towards the bulk as DMSO is added.

The first peak in the charge distributions can be directly related to the orientational ordering presented in the previous section. It can be seen how a thin positive layer is formed immediately next to the interfaces for both mixtures. This layer is created by the hydrogen atoms of the DMSO which, as can be seen in Fig. 4, favours orientations where its oxygen atom points towards the bulk.

The resulting charge profiles when the external electric field is activated are displayed in Fig. 8. It is evident that there is no notable variation between mixtures in this case, which again points to the fact that the presence of the electric fields overrides the hydrophobic effects present in the systems.

It is again possible to relate the charge layers closest to the walls to the orientation of the molecules that conform them. For both systems, a negative layer is seen next to the positive electrode, which is caused by DMSO molecules pointing their electronegative oxygen atoms towards the walls, in an attempt to balance electric charge, which can be seen in Fig. 5. On the other hand, the positive layer found next to the negatively charged interface is also due to DMSO molecules, which as seen in Fig. 6 have a preference to point their electropositive hydrogen atoms towards the interface, much like in the bulk mixtures. This orientation can even be seen in the snapshot represented in Fig. 3. Of course, in the case of

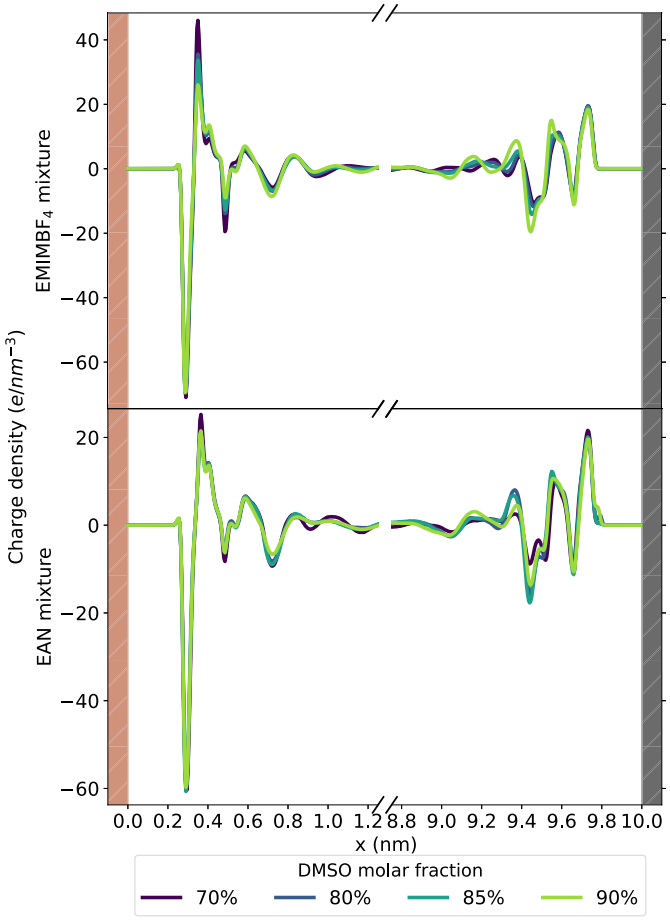

Fig. 8. Charge densities along the z-axis for both mixtures in the presence of an external field. Positive wall is red-coloured, negative wall is black-coloured.

the EAN mixtures, the occasional adsorption of metallic cations in the interfaces will also contribute to these positively charged structures.

It can be seen then that for all systems, both with and without an electric field, the charge distribution in the interfaces can be explained on the basis of the orientation of DMSO molecules. This is a direct consequence of their affinity for the interfaces, as evidenced by the density profiles in Figs. 1 and 2.

3.4. Electrostatic potential

The difference in electrostatic potential between the interfaces and the bulk can be found in Fig. 9. The potential at each point is calculated by direct integration of the Poisson equation, assuming that each individual point charge is smeared into a homogeneous planar distribution. This integration yields

$$\langle \phi(z) \rangle = -\frac{1}{\epsilon_0} \left\langle \sum_i q_i z_i \theta(z - z_i) \right\rangle, \tag{1}$$

where the sum runs over all particles in the system, ϵ_0 is the permitivity of free space, θ is the Heaviside step function and $\langle\rangle$ denotes the time-average. Bulk potentials were calculated by averaging the value of the electrostatic potential between 4 and 6 nm.

In Fig. 9a the potential of zero charge (i.e. the potential drop in absence of charge) is plotted. This takes relatively low values, ranging from 0.05 V to 0.4 V. In those systems, a clear difference can be seen between the protic and aprotic ILs. While for $EMIMBF_4$ the behaviour of the potential drop is smooth and exhibits a steady growth as DMSO concentration is increased, in the case of EAN a much more erratic behaviour can be seen. Although the potential drop seems to overall

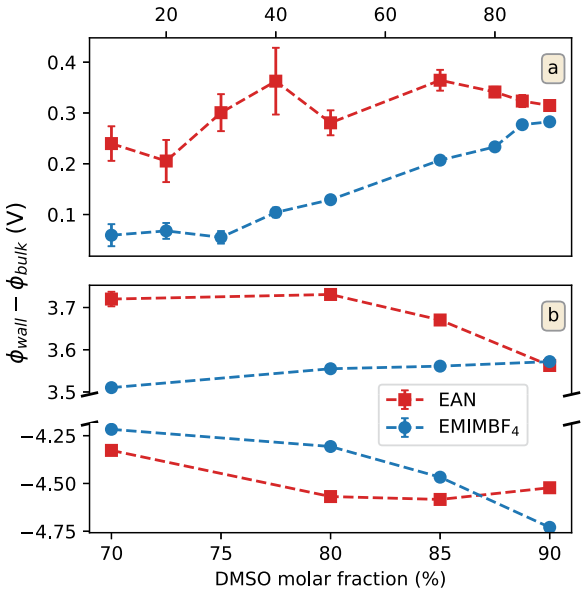

Fig. 9. Potential drop between the interfaces and the bulk for neutral (a) and charged (b) interfaces as a function of concentration. In the case of charged interfaces, the upper values represent the potential drop from the positive interface to the bulk, whereas the lower ones represent the potential drop from the negatively charged interface. Errorbars show the standard deviation of the bulk potential.

increase with DMSO concentration, it does so less smoothly than in the case of its aprotic counterpart. This could be due to the quasi-solid behaviour of EAN in the bulk region for low DMSO concentration, where the effects of the hydrogen bond network hold together the mixture hindering diffusion [38], thus resulting in the density oscillations seen in Fig. 1 and a less homogeneous potential. This is also reflected in the size of the errorbars, which reveal a greater standard deviation for the value of ϕ_{bulk}.

Remarkably, beyond a DMSO concentration of 70%, where the hydrogen bond network has been disrupted by the presence of the solvent, the addition of DMSO causes the potential drop to decrease in the case of EAN, while for $EMIMBF_4$ it continues to increase. It is also interesting to note that the potential drop is bigger for the protic IL throughout the whole concentration range. This can be related to the charge distributions seen in Fig. 7, where the charge layers near the interfaces are more pronounced in the case of EAN. The difference in the layering properties of each liquid, which in turn depends on the particular orientation of IL molecules near the interfaces, has an impact on the electrostatic potential, with higher charge concentrations near the electrodes resulting in a greater potential drop.

When an electric field is added, the behaviour of the potential drop changes depending on which interface one considers. In Fig. 9b it can be seen that the potential drop is larger for the negatively charged interface than in the positive one by a factor of 1 V, which can be attributed to the different composition of the molecular layers in each interface. Following the same trend as for the neutral interfaces, the magnitude of the potential drop seems to be greater for the protic IL, except for the 90% DMSO concentration mark, where $EMIMBF_4$ surpasses EAN. Moreover, it is important to note that the potential drop in the electropositive interface only varies about a quarter of a volt through the concentration range considered, whereas in the negatively charged interface, the potential drop encompasses a range between −4.2 V and −4.7 V.

Finally, the integral capacitance of the charged systems was calculated as $C = \rho/|\Delta\phi|$, with ρ the aforementioned 1 e/nm^2 charge density of the implicit electrodes. The results are shown in Table 1, where the total capacitance is represented, as well as the capacitances of both implicit interfaces, calculated from the potential drops in Fig. 9. The

Table 1
Capacitances of the charged systems.

	Integral Capacitance ($\mu F/cm^2$)		
	EAN		
	Positive-Negative	Positive-Bulk	Negative-Bulk
70% DMSO	1.991	4.307	3.703
80% DMSO	1.930	4.294	3.501
85% DMSO	1.941	4.365	3.496
90% DMSO	1.982	4.497	3.542
	$EMIMBF_4$		
	Positive-Negative	Positive-Bulk	Negative-Bulk
70% DMSO	2.073	4.564	3.799
80% DMSO	2.038	4.507	3.720
85% DMSO	1.996	4.499	3.587
90% DMSO	1.930	4.486	3.388

two interfaces show different capacitances, with the positive electrode displaying a higher one than the negative electrode for both ILs. The values obtained for the capacitance are similar to the ones obtained by Kislenko et al. [60] for $EMIMPF_6$, an aprotic IL similar to $EMIMBF_4$, in contact with graphene interfaces. The integral capacitance is larger for the aprotic IL except for the limiting case of very high DMSO concentrations, although the values of the capacitance for both ILs are relatively close to one another.

4. Conclusions

A study of the interfacial features of two ternary IL mixtures by means of MD simulations has been presented. Density distribution functions, orientational profiles, charge distribution and electrostatic potential of the mixtures when confined between implicit graphene walls were computed for several DMSO molar fractions. A protic IL (EAN) and an aprotic IL ($EMIMBF_4$) were selected in order to find the differences arising from the influence of hydrogen bond networks, a common feature in protic ILs due to the formation of proton donor and acceptor sites during their synthesis. Both cases of neutral and charged interfaces were simulated with the aim of identifying the effects arising from the activation of an electric field.

The density oscillations observed in the protic mixtures denote a hindered fluidification of the IL upon DMSO addition due to hydrogen bond networks precluding substitutions in ion solvation shells. Orientational profiles with uncharged walls show that chemical species either favour adopting orientations of maximal approach to the walls or that maximize the amount of hydrogen atoms facing them. Regarding metallic cations, the addition of DMSO is shown to favour the formation of structures near the interfaces, which in turn is reflective of enhanced Li^+ mobility, as seen in bulk simulations. The interfacial structures and orientations change upon charging of the walls, showing increased adsorption of densely charged and polar species. Analysis of the electrostatic potential revealed that the ability of Li^+ to reach the electrodes in the protic mixtures is unlikely to depend on the potential alone. Therefore, there is evidence that while the static properties of the system are mainly driven by the external potential, some dynamical features still depend on the molecular environment.

Overall, our results point at the fact that addition of DMSO is a beneficial approach for the utilization of the presented mixtures as electrolytes in electrochemical cells. Not only does it improve Li^+ transport numbers in the bulk, it also helps fluidification of the confined systems. Furthermore, orientations of the species near the walls are shown to be affected by the solvent concentration. The joined effects of this fluidification and the changes in orientations suggest a promotion of the appearance of paths for further approach of the metal ions to the electrodes upon addition of DMSO, specially in mixtures with protic ILs. This could be caused by a better mobility and greater ease for rearrangement under these conditions, as well as the smaller cation size in the protic IL.

The study presented here is another proof of the great differences among protic and aprotic IL mixtures. Hydrogen bond network formation and cation sizing result in generally differing behaviours. The authors had already observed this for the bulk properties and have now proved that the effect of these differences extends into the realm of interfacial properties. Activating the electric field reduces the influence of these differences in relation to the case of uncharged walls. However, our observations about the behaviour of metal cations suggest that they still can have an effect on phenomena that ultimately determine the performance of the mixture as an electrolyte, e.g. the ability of Li^+ to reach the electrodes. The interplay of the electrode-metal and electrolyte-metal interactions needs a proper modelling of the intricate electronic interactions present at the interface. Using a polarizable force field could help in the characterization of the lithium atom behaviour at the interface through the energy barrier. However, this method lacks the possibility of having true charge transfer between atoms that may be needed for an accurate description. Therefore methods like DFT or AIMD may be needed for a better understanding of this effect.

The results presented in this manuscript were obtained using the equivalent of a constant charge simulation. However, the results should not differ much from that obtained with constant potential methods, as it has been shown that, for planar electrodes, the general features of the structure remain mostly unchanged. Using constant potential simulations can lead to small changes on the distance of the first electrolyte layer to the electrode, and also to small changes in its width [61]. Using atomistic electrodes should also have minimal impact to the results. It has also been previously shown that the structure of the first layer close to the electrode shows the same features for implicit electrodes as that for pristine graphene [62].

5. Acknowledgements

The financial support of the Spanish Ministry of Science and Innovation (PID2021-126148NA-I00 funded by MCIN/AEI/10.13039/501100011033/FEDER, UE) are gratefully acknowledged. H. M. C. thanks the USC for his “Convocatoria de Recualificación do Sistema Universitario Español-Margarita Salas” postdoctoral grant under the “Plan de Recuperación Transformación” program funded by the Spanish Ministry of Universities with European Union’s NextGenerationEU funds. This work was supported by the Fundacão para a Ciência e Tecnologia (FCT) funded by national funds through the FCT/MCTES (PIDDAC)) to CIQUP, Faculty of Science, University of Porto (Project UIDB/00081/2020), IMS-Institute of Molecular Sciences (LA/P/0056/2020). T. M. M. acknowledges her contract funded by the pilot program of the USC for the recruitment of distinguished research personnel—call 2021 under the agreement between the USC and the Santander Bank for 2021–2024. M. O. L. and P. M. C. wish to thank the Xunta de Galicia for their “Axudas de apoio á etapa predoutoral” grants (ED481A 2022/236 and ED481A 2022/045).

CRediT authorship contribution statement

Martín Otero-Lema: Conceptualization, Formal analysis, Investigation, Methodology, Software, Validation, Visualization, Writing – original draft, Writing – review & editing. **Pablo Martínez-Crespo:** Conceptualization, Formal analysis, Investigation, Methodology, Software, Validation, Visualization, Writing – original draft, Writing – review & editing. **Trinidad Méndez-Morales:** Conceptualization, Funding acquisition, Investigation, Methodology, Supervision, Writing – original draft, Writing – review & editing. **Hadrián Montes-Campos:** Conceptualization, Investigation, Methodology, Supervision, Writing – original draft, Writing – review & editing. **Luis M. Varela:** Conceptualization, Funding acquisition, Methodology, Project administration, Supervision, Writing – original draft, Writing – review & editing.

Declaration of competing interest

The authors declare that they have no known competing financial interests or personal relationships that could have appeared to influence the work reported in this paper.

Data availability

Data will be made available on request.

References

[1] D.R. Easterling, J. Evans, P.Y. Groisman, T.R. Karl, K.E. Kunkel, P. Ambenje, Observed variability and trends in extreme climate events: a brief review, Bull. Am. Meteorol. Soc. 81 (3) (2000) 417–426.

[2] C.C. Ummenhofer, G.A. Meehl, Extreme weather and climate events with ecological relevance: a review, Philos. Trans. R. Soc. B, Biol. Sci. 372 (1723) (2017) 20160135.

[3] A. Kalair, N. Abas, M.S. Saleem, A.R. Kalair, N. Khan, Role of energy storage systems in energy transition from fossil fuels to renewables, Energy Storage 3 (1) (2021) e135.

[4] A. Kovač, M. Paranos, D. Marciuš, Hydrogen in energy transition: a review, Int. J. Hydrog. Energy 46 (16) (2021) 10016–10035.

[5] B. Chen, R. Xiong, H. Li, Q. Sun, J. Yang, Pathways for sustainable energy transition, J. Clean. Prod. 228 (2019) 1564–1571.

[6] A. Gallo, J. Simões-Moreira, H. Costa, M. Santos, E.M. Dos Santos, Energy storage in the energy transition context: a technology review, Renew. Sustain. Energy Rev. 65 (2016) 800–822.

[7] Y. Liang, C.-Z. Zhao, H. Yuan, Y. Chen, W. Zhang, J.-Q. Huang, D. Yu, Y. Liu, M.-M. Titirici, Y.-L. Chueh, et al., A review of rechargeable batteries for portable electronic devices, InfoMat 1 (1) (2019) 6–32.

[8] B.R. Chalamala, Portable electronics and the widening energy gap, Proc. IEEE 95 (11) (2007) 2106–2107.

[9] C.A. Pappijn, M. Ruitenbeek, M.-F. Reyniers, K.M. Van Geem, Challenges and opportunities of carbon capture and utilization: electrochemical conversion of CO_2 to ethylene, Front. Energy Res. 8 (2020) 557466.

[10] M. Rahimi, A. Khurram, T.A. Hatton, B. Gallant, Electrochemical carbon capture processes for mitigation of co2 emissions, Chem. Soc. Rev. 51 (2022) 8676–8695.

[11] S.E. Renfrew, D.E. Starr, P. Strasser, Electrochemical approaches toward CO_2 capture and concentration, ACS Catal. 10 (21) (2020) 13058–13074, https://doi.org/10.1021/acscatal.0c03639.

[12] J.N. Renner, L.F. Greenlee, K.E. Ayres, A.M. Herring, Electrochemical synthesis of ammonia: a low pressure, low temperature approach, Electrochem. Soc. Interface 24 (2) (2015) 51.

[13] Y. Huang, D.D. Babu, Z. Peng, Y. Wang, Atomic modulation, structural design, and systematic optimization for efficient electrochemical nitrogen reduction, Adv. Sci. 7 (4) (2020) 1902390.

[14] J. Yang, W. Weng, W. Xiao, Electrochemical synthesis of ammonia in molten salts, J. Energy Chem. 43 (2020) 195–207.

[15] A.R. Singh, B.A. Rohr, M.J. Statt, J.A. Schwalbe, M. Cargnello, J.K. Nørskov, Strategies toward selective electrochemical ammonia synthesis, ACS Catal. 9 (9) (2019) 8316–8324.

[16] A. Eftekhari, B. Fang, Electrochemical hydrogen storage: opportunities for fuel storage, batteries, fuel cells, and supercapacitors, Int. J. Hydrog. Energy 42 (40) (2017) 25143–25165.

[17] Z.P. Ifkovits, J.M. Evans, M.C. Meier, K.M. Papadantonakis, N.S. Lewis, Decoupled electrochemical water-splitting systems: a review and perspective, Energy Environ. Sci. 14 (2021) 4740–4759, https://doi.org/10.1039/D1EE01226F, https://doi.org/10.1039/D1EE01226F.

[18] D. Bedrov, J.-P. Piquemal, O. Borodin, A.D. MacKerell Jr, B. Roux, C. Schröder, Molecular dynamics simulations of ionic liquids and electrolytes using polarizable force fields, Chem. Rev. 119 (13) (2019) 7940–7995.

[19] E.J. Maginn, Atomistic simulation of the thermodynamic and transport properties of ionic liquids, Acc. Chem. Res. 40 (11) (2007) 1200–1207.

[20] E.J. Maginn, Molecular simulation of ionic liquids: current status and future opportunities, J. Phys. Condens. Matter 21 (37) (2009) 373101.

[21] H. Montes-Campos, A. Rivera-Pousa, T. Méndez-Morales, Density functional theory of alkali metals at the Li/graphene electrochemical interface, J. Chem. Phys. 156 (1) (2022) 014706, https://doi.org/10.1063/5.0077449, https://doi.org/10.1063/5.0077449.

[22] R.M. Lynden-Bell, M.G. Del Popolo, T.G. Youngs, J. Kohanoff, C.G. Hanke, J.B. Harper, C.C. Pinilla, Simulations of ionic liquids, solutions, and surfaces, Acc. Chem. Res. 40 (11) (2007) 1138–1145.

[23] M.C. Buzzeo, R.G. Evans, R.G. Compton, Non-haloaluminate room-temperature ionic liquids in electrochemistry—a review, Chem. Phys. Chem. 5 (8) (2004) 1106–1120.

[24] H. Liu, Y. Liu, J. Li, Ionic liquids in surface electrochemistry, Phys. Chem. Chem. Phys. 12 (8) (2010) 1685–1697.

[25] D.S. Silvester, R.G. Compton, Electrochemistry in room temperature ionic liquids: a review and some possible applications, Z. Phys. Chem. 220 (10) (2006) 1247–1274.

[26] K. Ghandi, A review of ionic liquids, their limits and applications, Green Sustain. Chem. (2014).

[27] M. Li, J. Lu, Z. Chen, K. Amine, 30 years of lithium-ion batteries, Adv. Mater. 30 (33) (2018) 1800561.

[28] O. Cabeza, S. García-Garabal, L. Segade, M. Domínguez-Pérez, E. Rilo, L.M. Varela, Physical properties of binary mixtures of ils with water and ethanol. A review, in: Ionic Liquids: Theory, Properties, New Approaches, 2011, pp. 111–136.

[29] A. Pal, M. Saini, B. Kumar, Volumetric, ultrasonic and spectroscopic (ft-ir) studies for the binary mixtures of imidazolium based ils with 1, 2-propanediol, Fluid Phase Equilib. 411 (2016) 66–73.

[30] H. Ning, M. Hou, Q. Mei, Y. Liu, D. Yang, B. Han, The physicochemical properties of some imidazolium-based ionic liquids and their binary mixtures, Sci. China Chem. 55 (8) (2012) 1509–1518.

[31] G. Raabe, J. Köhler, Thermodynamical and structural properties of binary mixtures of imidazolium chloride ionic liquids and alcohols from molecular simulation, J. Chem. Phys. 129 (14) (2008) 144503.

[32] M. Chen, R. Pendrill, G. Widmalm, J.W. Brady, J. Wohlert, Molecular dynamics simulations of the ionic liquid 1-n-butyl-3-methylimidazolium chloride and its binary mixtures with ethanol, J. Chem. Theory Comput. 10 (10) (2014) 4465–4479.

[33] H. Montes-Campos, J.M. Otero-Mato, T. Méndez-Morales, E. López-Lago, O. Russina, O. Cabeza, L.J. Gallego, L.M. Varela, Nanostructured solvation in mixtures of protic ionic liquids and long-chained alcohols, J. Chem. Phys. 146 (12) (2017) 124503.

[34] L. Varela, J. Carrete, M. García, L. Gallego, M. Turmine, E. Rilo, O. Cabeza, Pseudolattice theory of charge transport in ionic solutions: corresponding states law for the electric conductivity, Fluid Phase Equilib. 298 (2) (2010) 280–286.

[35] H. Montes-Campos, S. Kondrat, E. Rilo, O. Cabeza, L.M. Varela, Random-alloy model for the conductivity of ionic liquid–solvent mixtures, J. Phys. Chem. C 124 (22) (2020) 11754–11759.

[36] G.H. Lane, A.S. Best, D.R. MacFarlane, M. Forsyth, P.M. Bayley, A.F. Hollenkamp, The electrochemistry of lithium in ionic liquid/organic diluent mixtures, Electrochim. Acta 55 (28) (2010) 8947–8952, https://doi.org/10.1016/j.electacta.2010.08.023, https://www.sciencedirect.com/science/article/pii/S0013468610010856.

[37] K. Oldiges, D. Diddens, M. Ebrahiminia, J.B. Hooper, I. Cekic-Laskovic, A. Heuer, D. Bedrov, M. Winter, G. Brunklaus, Understanding transport mechanisms in ionic liquid/carbonate solvent electrolyte blends, Phys. Chem. Chem. Phys. 20 (2018) 16579–16591, https://doi.org/10.1039/C8CP01485J, https://doi.org/10.1039/C8CP01485J.

[38] P. Martínez-Crespo, M. Otero-Lema, O. Cabeza, H. Montes-Campos, L.M. Varela, Structure, dynamics and ionic conductivities of ternary ionic liquid/lithium salt/dmso mixtures, J. Mol. Liq. 359 (2022) 119188.

[39] A. Khan, C. Zhao, Enhanced performance in mixture DMSO/ionic liquid electrolytes: toward rechargeable Li–O_2 batteries, Electrochem. Commun. 49 (2014) 1–4, https://doi.org/10.1016/j.elecom.2014.09.014.

[40] K. Pranay Reddy, P. Fischer, M. Marinaro, M. Wohlfahrt-Mehrens, Improved Li–metal cycling performance in high concentrated electrolytes for Li-O_2 batteries, ChemElectroChem 5 (19) (2018) 2758–2766, https://doi.org/10.1002/celc.201800686.

[41] K. Fumino, A. Wulf, R. Ludwig, Hydrogen bonding in protic ionic liquids: reminiscent of water, Angew. Chem., Int. Ed. 48 (17) (2009) 3184–3186.

[42] K. Fumino, A. Wulf, R. Ludwig, The potential role of hydrogen bonding in aprotic and protic ionic liquids, Phys. Chem. Chem. Phys. 11 (39) (2009) 8790–8794.

[43] R. Hayes, S. Imberti, G.G. Warr, R. Atkin, The nature of hydrogen bonding in protic ionic liquids, Angew. Chem., Int. Ed. Engl. 125 (17) (2013) 4721–4725.

[44] N.-W. Li, Y.-X. Yin, J.-Y. Li, C.-H. Zhang, Y.-G. Guo, Passivation of lithium metal anode via hybrid ionic liquid electrolyte toward stable Li plating/stripping, Adv. Sci. 4 (2) (2017) 2–7, https://doi.org/10.1002/advs.201600400.

[45] M.J. Abraham, D. van der Spoel, E. Lindahl, B. Hess, The GROMACS Development Team, GROMACS User Manual version 2019, 2019, http://www.gromacs.org.

[46] W.L. Jorgensen, D.S. Maxwell, J. Tirado-Rives, Development and testing of the OPLS all-atom force field on conformational energetics and properties of organic liquids, J. Am. Chem. Soc. 118 (45) (1996) 11225–11236, https://doi.org/10.1021/ja9621760.

[47] W.L. Jorgensen, J. Tirado-Rives, The OPLS [optimized potentials for liquid simulations] potential functions for proteins, energy minimizations for crystals of cyclic peptides and crambin, J. Am. Chem. Soc. 110 (6) (1988) 1657–1666, https://doi.org/10.1021/ja00214a001.

[48] G. Bussi, D. Donadio, M. Parrinello, Canonical sampling through velocity rescaling, J. Chem. Phys. 126 (1) (2007) 014101.

[49] M. Parrinello, A. Rahman, Polymorphic transitions in single crystals: a new molecular dynamics method, J. Appl. Phys. 52 (12) (1981) 7182–7190.

[50] S. Nosé, M. Klein, Constant pressure molecular dynamics for molecular systems, Mol. Phys. 50 (5) (1983) 1055–1076.

[51] U. Essmann, L. Perera, M.L. Berkowitz, T. Darden, H. Lee, L.G. Pedersen, A smooth particle mesh Ewald method, J. Chem. Phys. 103 (19) (1995) 8577–8593.

[52] I.-C. Yeh, M.L. Berkowitz, Ewald summation for systems with slab geometry, J. Chem. Phys. 111 (7) (1999) 3155–3162.

[53] J.M. Otero-Mato, H. Montes-Campos, O. Cabeza, D. Diddens, A. Ciach, L.J. Gallego, L.M. Varela, 3d structure of the electric double layer of ionic liquid–alcohol

mixtures at the electrochemical interface, Phys. Chem. Chem. Phys. 20 (48) (2018) 30412–30427.

[54] L. Martínez, R. Andrade, E.G. Birgin, J.M. Martínez, Packmol: a package for building initial configurations for molecular dynamics simulations, J. Comput. Chem. 30 (13) (2009) 2157–2164.

[55] M.V. Fedorov, R.M. Lynden-Bell, Probing the neutral graphene-ionic liquid interface: insights from molecular dynamics simulations, Phys. Chem. Chem. Phys. 14 (8) (2012) 2552–2556, https://doi.org/10.1039/c2cp22730d.

[56] M.H. Miles, L.W. McMahon, S.M. Nelson, Electrochemical and transport properties of lithium chloride solutions in dimethyl sulfoxide-water and dimethyl sulfoxide-methanol mixtures, J. Phys. Chem. 79 (21) (1975) 2312–2315.

[57] V. Gómez-González, B. Docampo-Álvarez, J.M. Otero-Mato, O. Cabeza, L.J. Gallego, L.M. Varela, Molecular dynamics simulations of the structure of mixtures of protic ionic liquids and monovalent and divalent salts at the electrochemical interface, Phys. Chem. Chem. Phys. 20 (18) (2018) 12767–12776.

[58] N.N. Rajput, J. Monk, R. Singh, F.R. Hung, On the influence of pore size and pore loading on structural and dynamical heterogeneities of an ionic liquid confined in a slit nanopore, J. Phys. Chem. C 116 (8) (2012) 5169–5181.

[59] M. Alibalazadeh, M. Foroutan, Specific distributions of anions and cations of an ionic liquid through confinement between graphene sheets, J. Mol. Model. 21 (7) (2015) 1–10.

[60] S.A. Kislenko, I.S. Samoylov, R.H. Amirov, Molecular dynamics simulation of the electrochemical interface between a graphite surface and the ionic liquid [BMIM][PF6], Phys. Chem. Chem. Phys. 11 (27) (2009) 5584–5590, https://doi.org/10.1039/b823189c.

[61] C. Merlet, C. Péan, B. Rotenberg, P.A. Madden, P. Simon, M. Salanne, Simulating supercapacitors: can we model electrodes as constant charge surfaces?, J. Phys. Chem. Lett. 4 (2) (2013) 264–268.

[62] B. Docampo-Alvarez, V. Gomez-Gonzalez, O. Cabeza, V.B. Ivaništšev, L.J. Gallego, L.M. Varela, Molecular dynamics simulations of novel electrolytes based on mixtures of protic and aprotic ionic liquids at the electrochemical interface: structure and capacitance of the electric double layer, Electrochim. Acta 305 (2019) 223–231.